Microscopic description of the odd-even effect in cold fission

M. Mirea
Horia Hulubei National Institute for Physics and Nuclear Engineering, P.O. Box MG-G, Bucharest, Romania
(Received 29 September 2013; revised manuscript received 26 February 2014; published 26 March 2014)

The time-dependent equations of motion for the pair-breaking effect were corroborated with a condition that fixes dynamically the number of particles on the two-fission fragment. The single-particle level scheme was calculated with the Woods–Saxon superasymmetric two-center shell model. This model provides a continuous variation of the energies from one nucleus up to two separated fragments. The dissipated energy resorts from the time-dependent pairing equations. A peculiar phenomenon was observed experimentally in cold fission: the odd partition yields are favored over the even ones. This odd-even effect for cold fission was explained microscopically.

DOI: 10.1103/PhysRevC.89.034623 PACS number(s): 24.75.+i, 21.60.Cs, 24.10.Cn, 24.10.Eq

I. INTRODUCTION

By identifying unambiguously the fission fragments according to their mass number and their charge, the fission yields as function of the excitation energy were measured [1]. The experimental data showed a dominance of odd-odd fragments at excitation energies close to zero for U isotopes. This phenomenon was independently remarked also in Refs. [2,3] for Cf. A first interpretation involved a proportionality between the level densities of the fission fragments and the yields.

Recently, a new set of time-dependent coupled-channel equations derived from the variational principle was proposed to determine dynamically the mixing between seniority-zero and seniority-two configurations [4]. The essential idea is that the configuration mixing is managed under the action of some inherent low-lying time dependent excitations produced in the avoided-crossing regions; that is, a dynamical mechanism like the Landau–Zener effect [5].

In the pioneering investigations of the mass and charge distributions at low excitation energies, the experimental results showed a preference for the mass division leading to even-Z fragments [6,7]. It was believed that, at very low excitation energies, i.e., high kinetic energies, the fragments would be fully paired. Improving the experimental procedure, these facts were contradicted in Ref. [8] where no strong even-odd effect was evidenced in the thermal neutron induced fission for high values of the total kinetic energy. Even and odd partitions were observed experimentally close to their respective Q values for the four systems investigated: ^{233,235}U(n$_{th}$,f), ^{239}Pu(n$_{th}$,f) and ^{252}Cf(sf). It is worth underlining that the importance of the Landau–Zener effect in the cold-fission fragmentation behavior was anticipated, as mentioned in Ref. [9]. However, the odd-even structure in fission is explained usually within statistical arguments, as for example in Refs. [10–13]. Recently, some arguments linked the odd-even structure also to the charge asymmetry evolution during the fission process [14,15], not only to the dissipated energy as has been done earlier [16,17].

II. FORMALISM

In this section, the ingredients required to investigate dynamically the odd-even effect are described.

A. Equations of motion

The usual theories of fission consider that the nuclear system is characterized by several generalized coordinates $q(t) = \{q_n(t)\}$, $(n = 1, \ldots, N)$. These coordinates vary and force the system to split into two separated fragments. The single-particle energies, and the many-body wave function are determined by the the variation in time of these coordinates. In order to deduce the microscopic equations of motion, the starting point is a many-body Hamiltonian with pairing residual interactions:

$$H(q_i(t)) = \sum_{k>0} \epsilon_k(q_i(t))(a_k^+ a_k + a_{\bar{k}}^+ a_{\bar{k}}) - \sum_{k,l>0} G_{kl}(t) a_k^+ a_{\bar{k}}^+ a_l a_{\bar{l}}. \quad (1)$$

This Hamiltonian depends on the collective parameters $q(t)$, which are allowed to vary with respect the time. Here, ϵ_k are single-particle energies, and a_k^+ and a_k denote operators for creating and destroying a particle in the state k, respectively. The state characterized by a bar signifies the time-reversed partner of a pair. The pairing correlations arise from the short-range interaction of correlated pairs of fermions moving in time-reversed orbits. G_{kl} is the matrix element of the pairing interaction and its value is in principle dependent on the overlap of the wave functions of the pairs. For a given nucleus, it is possible to approximate the pairing interaction matrix elements with a constant value by using a renormalization procedure that depends on the number of states in the active pairing space and on the structure [18].

Concerning the pair-breaking effect, it must be evidenced that only two types of velocity-dependent excitation mechanisms are possible between different single-particle (or molecular) states of a dynamical nuclear system [19]: the radial coupling that can be described by the Landau–Zener effect in avoided-level-crossing regions and the Coriolis one produced in the region of real crossings. The Coriolis coupling is responsible for transitions between levels characterized by quantum numbers of the projection of the spin that differ by one unity. This coupling is important in the treatment of the α decay where the inertia is small, and such an investigation was made in Ref. [20]. Concerning the dynamical pair breaking, it

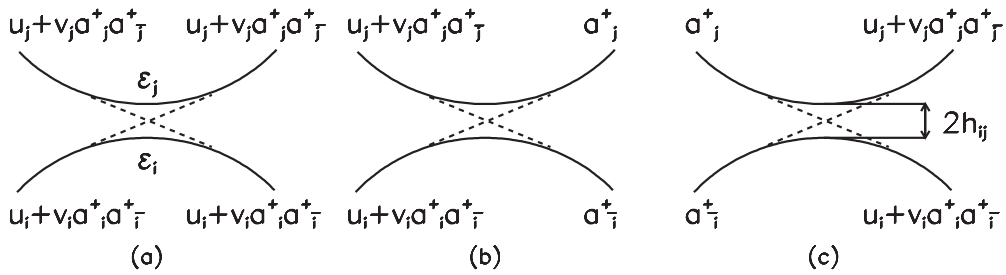

FIG. 1. Ideal avoided-crossing regions between two adiabatic single- particle levels ϵ_i and ϵ_j characterized by the same good quantum numbers. Three possible transitions between configurations in an avoided-crossing region in the superfluid model are displayed: (a) The configuration remains unchanged after the passage through the avoided-crossing region. (b) A pair is broken. (c) A pair is created.

can be described by a mechanism similar to the Landau–Zener one. The perturbation that produces the pair breaking in avoided-crossing regions between levels with the same good quantum numbers is obtained in terms of quasiparticle creation and annihilation operators

$$\begin{aligned} \alpha_{k(ij)} &= u_{k(ij)}a_k - v_{k(ij)}a^+_{\bar{k}}, \quad \alpha_{\bar{k}(ij)} = u_{k(ij)}a_{\bar{k}} + v_{k(ij)}a^+_k, \\ \alpha^+_{k(ij)} &= u_{k(ij)}a^+_k - v^*_{k(ij)}a_{\bar{k}}, \quad \alpha^+_{\bar{k}(ij)} = u_{k(ij)}a^+_{\bar{k}} + v^*_{k(ij)}a_k. \end{aligned} \tag{2}$$

Within the previous transformations, some perturbations that break dynamically a Cooper pair when the system traverses an avoided-level-crossing region are constructed. The parameters $v_{k(ij)}$ and $u_{k(ij)}$ are occupation and vacancy amplitudes, respectively, for a pair occupying the single-particle level k of the configuration $\{ij\}$. The seniority-zero configuration is denoted with 0 and the seniority-two configuration by a pair of indexes $\{ij\}$, i and j denoting the levels occupied by unpaired fermions. As evidenced in Ref. [4], the three situations plotted in Fig. 1 can be modeled. In the plot of Fig. 1(a), the Cooper pair remains on the adiabatic level ϵ_j, in Fig. 1(b) the pair destruction is illustrated, while in Fig. 1(c) two fermions generate a pair. To describe these three situations, a residual perturbation in the avoided-level-crossing region is postulated as follows:

$$H'(t) = \sum_{i,j\neq i}^{n} h_{ij}(t) \left[\alpha_{i(0)}\alpha_{\bar{j}(0)} \prod_{k\neq i,j} \alpha_{k(0)}\alpha^+_{k(ij)} + \alpha^+_{i(0)}\alpha^+_{\bar{j}(0)} \prod_{k\neq i,j} \alpha_{k(ij)}\alpha^+_{k(0)} \right], \tag{3}$$

where h_{ij} is the interaction energy between levels in the avoided-level-crossing regions. Under the action of the interaction h_{ij}, according to the identities (A5) of the Appendix, the operators $\alpha_{i(0)}\alpha_{\bar{j}(0)}$ and $\alpha^+_{i(0)}\alpha^+_{\bar{j}(0)}$ transform a Bogoliubov seniority-zero wave function into a seniority-two wave function, and vice versa, being responsible for configuration mixing. The products over the index $k \neq i, j$ in the previous formula transform the remaining Bogoliubov amplitudes from values pertaining to the seniority-zero wave function to those pertaining to the seniority-two functions with unpaired orbitals i and j, and vice versa. This dynamical pair-breaking effect was theoretically formulated in Ref. [4] for the first time. It is important to note that the same kind of perturbation was used also to generalize the Landau-Zener effect in superfluid systems [21–23]. It was demonstrated in Ref. [21] that equations governing the Landau–Zener effect and the time-dependent pairing equations are two particular cases of a new set of coupled-channel equations.

The two fission products must be characterized by integer numbers of neutrons and protons. As a consequence, the sums of the occupation probabilities of single-particle levels of the two fragments must give the mass and charge numbers. By solving the equations of motion, unfortunately, the sum of single-particle densities (BCS occupation probabilities) of the single-particle levels belonging to the two fission fragments obtained after the scission do not give exactly their numbers of nucleons. A recipe can be implemented to fix dynamically these numbers of particles in the two final fragments by using the operators for the number of particles $\hat{N}_i$ $(i = 1,2)$ that act on each fission product. At scission, the two fission fragments must be characterized by a supplementary condition

$$|N_2\hat{N}_1 - N_1\hat{N}_2| = 0, \tag{4}$$

where N_1 and N_2 are the number of particles in the final fragments labeled 1 and 2, respectively, and

$$\hat{N}_1 = \sum_{k1} \left(a^+_{k_1}a_{k_1} + a^+_{\bar{k}_1}a_{\bar{k}_1}\right), \quad \hat{N}_2 = \sum_{k2} \left(a^+_{k_2}a_{k_2} + a^+_{\bar{k}_2}a_{\bar{k}_2}\right) \tag{5}$$

are the corresponding operators. Here, k_1 and k_2 run over the pairing active level states that are located in the potential wells of the final fragment 1 and of the final fragment 2, respectively. The condition (4) can be introduced in the equations of motion by means of the Lagrange multipliers [24,25].

All the previous ingredients could be used to obtain the microscopic equations of motion. These equations are obtained from the variational principle by minimizing the following energy functional:

$$\delta\mathcal{L} = \delta\langle\varphi|H + H' - \lambda|N_2\hat{N}_1 - N_1\hat{N}_2| - i\hbar\frac{\partial}{\partial t}|\varphi\rangle. \tag{6}$$

The trial many-body function φ is a superposition of Bogoliubov seniority-zero and seniority-two wave functions:

$$|\varphi(t)\rangle = \left[c_0 \prod_k (u_{k(0)}(t) + v_{k(0)}(t)a^+_k a^+_{\bar{k}}) + \sum_{j,l\neq j} c_{jl}(t)a^+_j a^+_{\bar{l}} \times \prod_{k\neq j,l} (u_{k(jl)}(t) + v_{k(jl)}(t)a^+_k a^+_{\bar{k}}) \right] |0\rangle, \tag{7}$$

where c_0 is the amplitude of the seniority-zero wave function while c_{jl} are amplitudes for the seniority-two wave functions for configurations in which the single-particle orbitals j and

l belonging to the active pairing space are each blocked by only one unpaired nucleon. Here, the vacancy u_k and occupation v_k amplitudes are not the adiabatic solutions of the BCS equations and depend on the variation in time of the generalized parameters and the history of the nuclear system. λ is a Lagrange multiplier.

The evolution in time of the nuclear system, if the collective parameters $\{q_n(t)\}$ ($n = 1, \ldots, N$) vary, is obtained by performing the variation of the functional (6). The procedure required for the functional variation is described in detail in the Appendix. The next coupled-channel equations are obtained, eventually:

$$i\hbar\dot{\rho}_{k(0)} = \kappa_{k(0)}\Delta^*_{k(0)} - \kappa^*_{k(0)}\Delta_{k(0)}, \tag{8}$$

$$i\hbar\dot{\rho}_{k(jl)} = \kappa_{k(jl)}\Delta^*_{k(jl)} - \kappa^*_{k(jl)}\Delta_{k(jl)}, \tag{9}$$

$$i\hbar\dot{\kappa}_{k(0)} = (2\rho_{k(0)} - 1)\Delta_{k(0)} + 2\kappa_{k(0)}\left(\epsilon_k - sN_{i_k}\lambda\right) - 2G_{kk}\rho_{k(0)}\kappa_{k(0)}, \tag{10}$$

$$i\hbar\dot{\kappa}_{k(jl)} = (2\rho_{k(jl)} - 1)\Delta_{k(jl)} + 2\kappa_{k(jl)}\left(\epsilon_k - sN_{i_k}\lambda\right) - 2G_{kk}\rho_{k(jl)}\kappa_{k(jl)}, \tag{11}$$

$$i\hbar\dot{P}_0 = \sum_{l,j\neq l} h_{lj}(S^*_{0jl} - S_{0jl}), \tag{12}$$

$$i\hbar\dot{P}_{jl} = h_{lj}(S_{0jl} - S^*_{0jl}), \tag{13}$$

$$i\hbar\dot{S}_{0jl} = S_{0jl}(\bar{E}_0 - \bar{E}_{jl}) + S_{0jl}\left(\sum_{k\neq j,l} T_{k(jl)} - \sum_k T_{k(0)}\right) + \sum_{\{mn\}\neq\{jl\}} h_{mn}S_{mnjl} + h_{jl}(P_{jl} - P_0), \tag{14}$$

$$i\hbar\dot{S}_{mnjl} = S_{mnjl}(\bar{E}_{mn} - \bar{E}_{jl}) + S_{mnjl}\left(\sum_{k\neq m,n} T_{k(mn)} - \sum_{k\neq j,l} T_{k(jl)}\right) + h_{mn}S_{0jl} - h_{jl}S^*_{0mn}, \tag{15}$$

where j, k, l, m, n label the single-particle levels in the active pairing space. The sign $s = \pm 1$ ensures that the matrix element of the expression (4) is positive. $N_{i_k} = N_2$ or $N_{i_k} = -N_1$ if the state k will be located in the fragment 1 or in the fragment 2 after the scission, respectively. Here, the following notations are used:

$$\begin{aligned}
\Delta_{k(0)} &= \sum_{k'} \kappa_{k'(0)}G_{kk'}, \quad \Delta_{k(jl)} = \sum_{k'\neq j,l} \kappa_{k'(jl)}G_{kk'},\\
\kappa_{k(0)} &= u_{k(0)}v_{k(0)}, \quad \rho_{k(0)} = |v_{k(0)}|^2,\\
\kappa_{k(jl)} &= u_{k(jl)}v_{k(jl)},\\
\rho_{k(jl)} &= |v_{k(jl)}|^2, \quad P_0 = |c_0|^2, \quad P_{jl} = |c_{jl}|^2,\\
S_{0jl} &= c_0c^*_{jl}, \quad S_{mnjl} = c_{mn}c^*_{jl}.
\end{aligned} \tag{16}$$

The symbol Δ_γ gives the gap parameter. (The label γ denotes here generically a specific configuration.) The variables that depend on time through the generalized coordinates are the single-particle densities ρ_γ, the pairing moment components κ_γ, the probabilities to have a given seniority configuration P_γ, and the moment components between configurations $S_{\gamma\gamma'}$. The relations (8)–(12) are the well-known time-dependent paring equations previously deduced in Refs. [26,27]. These formulas are identical to the time dependent Hartree–Fock–Bogoliubov equations [28,29]. The symbol h_γ denotes the Landau–Zener interaction, while $\bar{E}_\gamma$ and T_γ are energy terms. The significance of the quantities appearing in the equations can be understood in the Appendix. The condition that $\sum_\gamma P_\gamma = 1$ is implicitly ensured through Eqs. (12) and (13) because $\dot{P}_0 + \sum_\gamma \dot{P}_\gamma = 0$.

B. Dissipation

The energy of the nuclear system in the seniority-zero state is

$$\begin{aligned}
E_0 &= \left\langle \prod_k [u_{k(0)}(t) + v_{k(0)}(t)a^+_k a^+_{\bar{k}}] | H | \prod_k [u_{k(0)}(t) + v_{k(0)}(t)a^+_k a^+_{\bar{k}}] \right\rangle\\
&= 2\sum_k \rho_{k(0)}\epsilon_k - \sum_k \kappa_{(0)} \sum_{k'} \kappa^*_{k'(0)}G_{kk'} - \sum_k \rho^2_{k(0)}G_{kk},
\end{aligned} \tag{17}$$

and in the seniority-two state it is

$$\begin{aligned}
E_{jl} &= \left\langle a^+_j a^+_{\bar{l}} \prod_{k\neq j,l} [u_{k(jl)}(t) + v_{k(jl)}(t)a^+_k a^+_{\bar{k}}] | H | a^+_j a^+_{\bar{l}} \prod_{k\neq j,l} [u_{k(jl)}(t) + v_{k(jl)}(t)a^+_k a^+_{\bar{k}}] \right\rangle\\
&= 2\sum_{k\neq j,l} \rho_{k(jl)}\epsilon_k - \sum_{k\neq j,l} \kappa_{k(jl)} \sum_{k'\neq j,l} \kappa^*_{k'(jl)}G_{kk'} - \sum_{k\neq j,l} \rho^2_{k(jl)}G_{kk} + \epsilon_j + \epsilon_l.
\end{aligned} \tag{18}$$

The corresponding lower-energy states E^0_0 and E^0_{jl} of the nuclear system in a given configuration are obtained with the previous relations by replacing the densities ρ_γ and the pairing moment components κ_γ with the adiabatic values obtained in the BCS approximation and using the same single-particle-level scheme. Consequently, as defined in Ref. [26], along the fission path the average dissipated energies E^*_γ will be

$$E^*_0 = E_0 - E^0_0, \quad E^*_{jl} = E_{jl} - E^0_{jl}, \tag{19}$$

in the seniority-zero and the seniority-two configurations, respectively. From the total potential energy of the nuclear system, we subtracted its adiabatic value. It was already shown in Ref. [30] that the mean value of the dissipated

energy becomes larger when the velocities of the generalized coordinates increase.

The single-particle levels belonging to the core of the initial parent nucleus are rearranged in the two cores of the fragments. Knowing the number of levels in each core, it is possible to redefine the pairing active space of each fragment and the asymptotic values of the lower-energy states can be evaluated. After the scission, E_0^0 must be replaced by the sum $E_{10}^0 + E_{20}^0$, where E_{10}^0 and E_{20}^0 are the lower energies of the two fission fragments. A similar rule is valid also for seniority-two configurations. At the same time, the pairing interaction matrix elements $G_{kk'}$ between pairs pertaining to different nuclei are zero. For each channel, asymptotically [24], the next limits hold

$$E_0^0 \to E_{10}^0 + E_{20}^0, \quad E_{0jl}^0 \to E_{1jl}^0 + E_{2jl}^0, \tag{20}$$

where the indices 1 and 2 refer to the two fragments. If only one pair is broken along the fission path, the spin of the two nuclei delivered from one unique seniority-two configuration must be the same. This last assumption is due to the fact that the Landau–Zener effect is produced between levels with the same good quantum numbers.

C. Macroscopic-microscopic method and single-particle energies

In order to determine the fission barriers, the total energy of the nuclear system is computed in the framework of the macroscopic-microscopic method [18,31]. As mentioned previously, the whole system is characterized by some collective coordinates that determine approximately the behavior of many other intrinsic variables. The essential idea of this approach is that a macroscopic model, such as the liquid-drop model, describes quantitatively the smooth trends of the potential energy with respect the particle number and deformation, whereas a microscopic approach such as the shell model describes local fluctuations. The combined macroscopic-microscopic method should reproduce both smooth trends and local fluctuations. The basic ingredient in such an analysis is the shape parametrization that depends on several macroscopic degrees of freedom. The macroscopic deformation energy is calculated within the liquid-drop model. A microscopic potential must be constructed to be consistent with this nuclear shape parametrization. A microscopic correction is then evaluated using the Strutinsky procedure [32].

The basic ingredient of the model is the nuclear shape parametrization. In the following, an axial symmetric nuclear shape surface during the deformation process from one initial nucleus to the separated fragments is obtained by smoothly joining two spheroids of semi-axes a_i and b_i $(i = 1, 2)$ with a neck surface generated by the rotation of a circle of radius R_3 around the axis of symmetry. By imposing the condition of volume conservation we are left with five independent generalized coordinates $\{q_n\}$ $(n = 1, 5)$ that can be associated with five degrees of freedom: the elongation R given by the distance between the centers of the spheroids, the necking parameter $C = S/R_3$ related to the curvature of the neck, the eccentricities ϵ_i associated with the deformations of the nascent fragments, and the mass asymmetry parameter

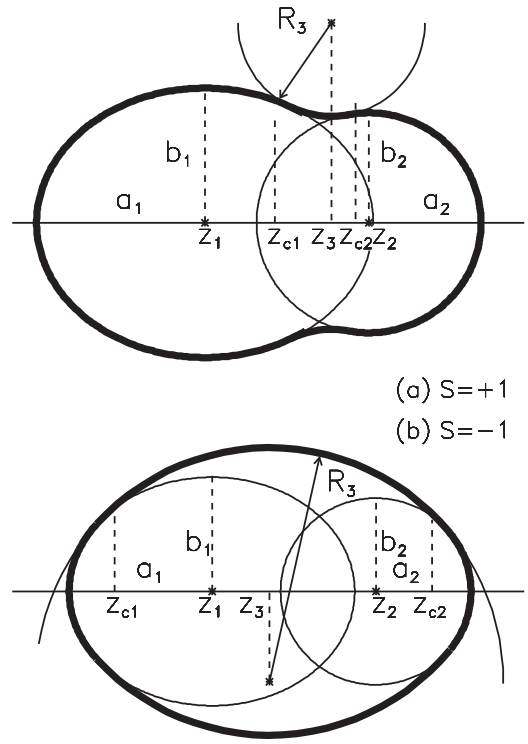

FIG. 2. Nuclear shape parametrization. The elongation is defined as $R = z_2 - z_1$. The curvature of the neck parameter is $C = S/R_3$, where $S = 1$ for necked shapes in the median surface and $S = -1$ otherwise. The eccentricities of the fragments are $\epsilon_i = \sqrt{1 - (b_i/a_i)^2}$ $(i = 1,2)$. The mass asymmetry parameter can be defined as $\eta = a_1 b_1^2/(a_2 b_2^2)$.

$\eta = V_1/V_2$, V_i $(i = 1, 2)$ denoting the volumes of the virtual ellipsoids characterized by the semi-axes a_i and b_i. The nuclear shape parametrization is displayed in Fig. 2. The entire model can be considered valid as long as the generalized coordinates and their variations in time make sense.

The many-body wave function and the single-particle energies are provided by the Woods–Saxon two-center shell model [21]. The Woods–Saxon potential, the Coulomb interaction, and the spin-orbit term must be diagonalized in an eigenvector basis. The asymmetric two-center shell oscillator provides an orthogonal eigenvector basis for only one Hermite space [33,34]. In this Hermite space the behavior of both fragments can be described. When the elongation R is zero, the eigenvector basis becomes that of the anisotropic oscillator. When R tends to infinity, a two-oscillator eigenvector system is obtained in the same Hermite space, centered in the two fragments. In the intermediate situation, each eigenfunction has components in the two subspaces that belong to the fragments. So, the two-center shell model provides permanently the wave functions associated to the lower energies of the single-particle states pertaining to a major quantum number $N_{\max}$. Therefore, molecular states formed by two fragments at scission could be precisely described. Another feature of the two-center shell model is related to the localization of the single-particle wave function in one of the two potential wells after the scission. As evidenced in Ref. [24], it is possible to predict this localization

for a given fragmentation before that the scission is produced. This feature helps us to fix the number of particles in each fragment by resolving Eqs. (8)–(16).

This model was widely used by the Bucharest group in the calculations addressing the cluster [35–39] and α decay [40], the fission [41–43], or the heavy-element synthesis [44]. For example, the model was able to describe two tangent nuclei in a wide range of mass asymmetries. The half-lives for cluster decay were reproduced. A mechanism for the formation of an α particle on the nuclear surface was supplied. Fission barriers that agree with the evaluated ones were calculated.

If the different penetrabilities which characterize every channel through the barrier are taken into account, it is expected that the daughter ground state is strongly enhanced in the exit channel. Indeed, in the cases of the excited channels, the barrier must be increased with approximately the value of the excitation energy of the unpaired nucleon and, therefore, the penetrability is decreased exponentially. The amount of which the barrier is modified can be estimated by accounting for the specialization energy. Wheeler defined this specialization energy [45] as the excess of the energy of a nucleon with a given spin over the energy for the same spin nucleon state of lowest energy. So, the final excitation is given by the sum between the dissipated energy and the single-particle excitations that are equivalent to the specialization energies.

The probability to obtain a given partition in the mass distribution is determined by the penetrability of the fission barrier:

$$P_b = \exp\left\{-\frac{2}{\hbar}\int_{r_a}^{r_b}\sqrt{B(r)[V(r)-U]}dr\right\}. \qquad (21)$$

The exponent is the classical action integral taken along the fission path at a given energy U that connects the two turning points $r_a(U)$ and $r_b(U)$. Only positive values of $[V(r)-U]$ are integrated. B is the inertia along the fission trajectory and V is the deformation energy.

III. RESULTS

The fission yields as function of the total excitation energy for the fragmentation ^{90}Kr + ^{144}Ba (even-even), ^{90}Rb + ^{144}Cs (odd-odd) will be investigated in the framework of our model. Experimental data are available for the reaction [1] ^{233}U(n$_{\rm th}$,f) and the model can be tested.

In order to determine the rearrangement of the single-particle energies, the first step is the calculation of the fission path from the ground state up to scission. As described in Ref. [42], the minimal action principle can be used to determine the best fission trajectory in the configuration space spanned by our five generalized coordinates. For this purpose, two ingredients are required: the deformation energy V and the tensor of the effective mass $\{B_{ij}\}$. The deformation energy was obtained in the frame of the microscopic-macroscopic method. The effective mass is computed within the cranking approximation. By minimization, the theory can give us the most probable fragmentation, that corresponds to a heavy fragment with mass around 138. In our work, the fission path for the 144/90 fragmentation is required. As evidenced in Ref. [46], it is not yet understood how the compound nucleus is transformed in a variety of different fragmentations. It is also believed that the models for mass distributions have limited predictive power. To overcome these difficulties, some simple assumptions are made in our work. We rely on the results of Refs. [25,41] where the mass distribution of the fragments was relatively well reproduced by considering that the variation of the mass asymmetry is linear from the saddle configuration of the outer barrier up to the exit point. It is considered that under the rapid descent from the top of the second barrier different mass partitions are obtained. To obtain these different mass partitions, the simplest way is to vary the mass asymmetry parameter η and the averaged deformations of fragments as in Ref. [25]. The fission barrier is plotted in Fig. 3 for the partition $A_1/A_2 = 144/90$. At $R \approx 17$ fm, the variation of the mass asymmetry parameter is started, producing a small bump in the barrier. In Fig. 3(b), the effective mass is displayed. The inertia along the trajectory was computed with three approximations: the nonadiabatic cranking model [47,48], the Gaussian overlap approximation [49,50], and the cranking approach [5]. In order to solve the equations of motion, we need the single-particle energies, the variations of the pairing matrix elements G_{kl}, the interactions in the avoided-crossing regions, and the velocity of passage through these regions.

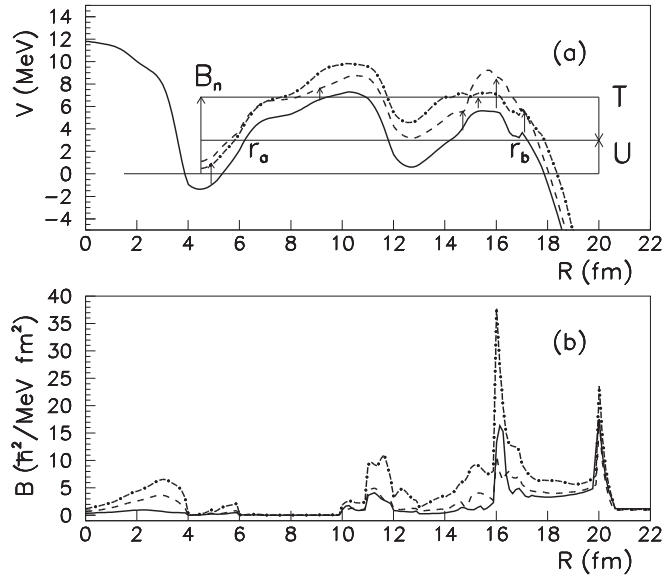

FIG. 3. (a) The fission barrier is plotted with a full line. The lower single-particle excited seniority-two state for neutrons is plotted with a dot-dashed line while the first one for protons is plotted with a dashed line. The avoided-level-crossing regions are marked with arrows. The turning points r_a and r_b are defined for a given collective potential energy U. (b) The inertia in the nonadiabatic cranking approximation is plotted with a full line, the inertia within the Gaussian overlap approximation is plotted with a dashed line, and the inertia in the cranking approximation is plotted with a dot-dashed line.

In Figs. 4 and 5, the single-particle energy levels obtained within the two-center Woods–Saxon model are displayed along the fission trajectory for neutrons and protons, respectively. With a dashed thick line the Fermi levels of the parent

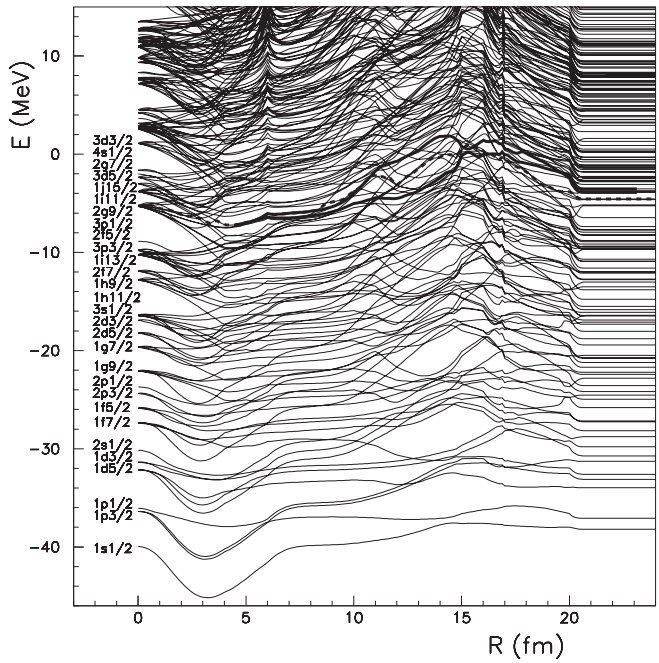

FIG. 4. Neutron single-particle-level scheme. The levels with spin projection $\Omega = 5/2$ that give the lower-energy configuration for the unpaired fragments are plotted with a full line. The Fermi energy of the compound nucleus is displayed with a thick dashed line. Four avoided-level-crossing regions were identified for $R \approx 4.9$, 15.3, 17.1, and 19.6 fm.

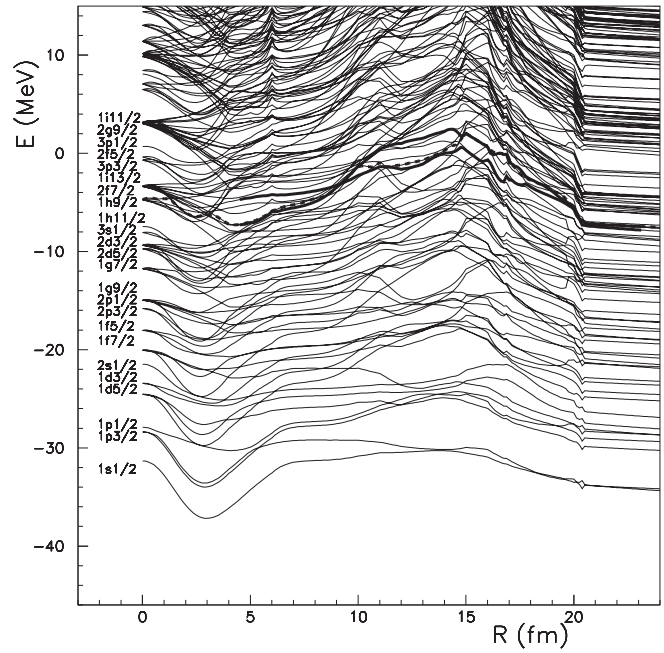

FIG. 5. Proton single-particle-level scheme. The levels with spin projection $\Omega = 3/2$ that give the lower-energy configuration for the unpaired fragments are plotted with a full line. The Fermi energy of the compound nucleus is displayed with a thick dashed line. Four avoided-level-crossing regions were identified for $R \approx 9.1$, 14.7, 16, and 20 fm.

nucleus are plotted. The pair of levels with the same spin projection that gives the lower single-particle seniority-two excitation (or specialization energy) are also displayed with thick full lines. It can be observed that the levels that pertain to the lower excitation are close to the Fermi energy. In the case of protons the spin projection Ω of these levels is $3/2$ while in the case of neutrons it is $\Omega = 5/2$. These values of Ω give also the final spin of the partners. The barriers for the seniority-two configurations were displayed in Fig. 3 with dot-dashed and dashed lines. The difference between the seniority-two and seniority-zero energies, that is the single-particle excitations, are obtained by subtracting their values computed with Eqs. (18) and (17) and by using the adiabatic BCS amplitudes. Our pairing active space is constructed with 58 single-particle levels around the Fermi energy.

An important question is the identification of the avoided-crossing regions that arise from the strong energy fluctuations of the single-particle levels observed along the fission path. For this purpose, we selected all the pairs of adjacent levels with the same spin projection in the active pairing space. From an analysis of the rearrangement of these levels in a manner similar to that of Ref. [51], the avoided-crossing regions were identified. The positions of some avoided-level-crossing regions are marked with arrows in Fig. 3. In these regions, the excitations are possible between the mentioned seniority-two configurations and the seniority-zero one. In other words, these regions are like gates for mixing the configurations, or for changing the seniority. Using the interpolation method described in Ref. [52], the magnitude of the interactions was calculated. Finally, we selected 32 seniority-two configurations for protons and 31 configurations for neutrons that are coupled to the seniority-zero configuration through avoided-level-crossing regions. In the frame of the adiabatic BCS model [5], a mean value of the pairing interaction G can be associated with a given active pairing space, by using a renormalization procedure. So, the values of G for all seniority states were computed for the parent and for the two fragments. In the case of seniority-two states, the blocked levels are eliminated from the single-particle diagram. A linear interpolation between the values of G from those of the parent to those of the fragments is realized in order to solve the equations of motion, as will be specified in the following. So, all the most important quantities required to solve the equations of motion are provided: the single-particle energies ϵ_k, the perturbations h_{ij}, and the pairing interactions G. The dependence in time is introduced by means of the variations of the collective coordinates. In this respect, several values of the internuclear velocity $v = \dot{R}$ are tested in order to solve the equations: 5×10^2, 8×10^2, 10^3, 3×10^3, 10^4, 3×10^4, 10^5, 3×10^5, 10^6, and 3×10^6 fm/fs.

Equations (8)–(12) do not have a dependence on P_γ and $S_{\gamma\gamma'}$ and can be solved separately for different values of the internuclear velocities. The initial conditions are given by the adiabatic BCS values for the ground-state deformation of the parent (located at $R \approx 4.6$ fm) of all seniority states involved. The equations are solved in a way similar to that presented in Ref. [24]. That is, at the beginning of the reaction

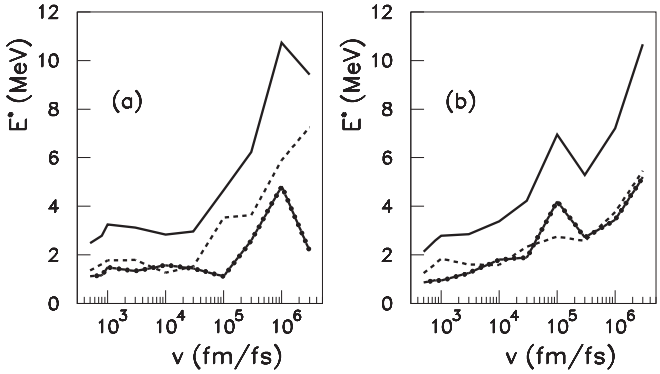

FIG. 6. (a) Total dissipation energy after the scission E^* as function of the internuclear velocity v for the seniority-zero configuration. The neutron and proton components of the dissipated energy are plotted with a dot-dashed and a dashed line, respectively. (b) Total dissipation for the seniority-two configuration with lower single-particle excitation. The neutron and proton components are displayed with the same line types as in panel (a).

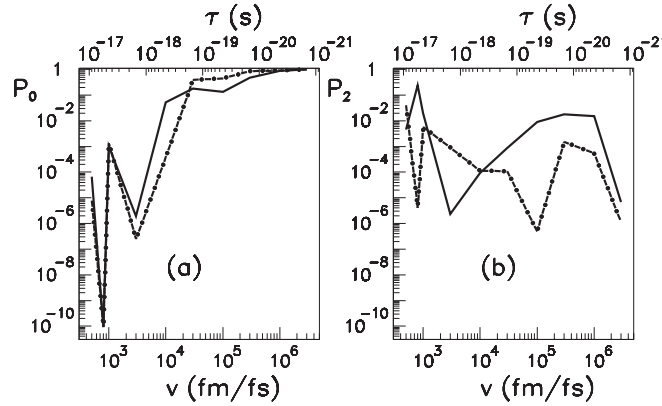

FIG. 7. (a) Probability of realization of the adiabatic seniority-zero configuration at scission as function of the internuclear velocity for neutrons (full line) and protons (dot-dashed line). (b) Probability of the realization of the seniority-two configuration at scission with the lower single-particle excitation for neutrons (full line) and protons (dot-dashed line). The upper axis corresponds to the saddle-to-scission time τ.

the system evolves without constraints. At the internuclear distance $R = 17$ fm, close to the top of the outer barrier, in Eqs. (11) and (12) the value of λ is set to nonzero values. At the same time, two linear variations of the mean value of the pairing interactions G are started in order to reach the final values G_1 and G_2 that characterize the two fragments at scission. When the equalities between the sums of single-particle occupation probabilities and the numbers of nucleons are obtained, λ and the pairing interaction between the two fragments G_{12} are set to zero. For $G_{12} = 0$, from conservation conditions as explained in Ref. [24], the sum of occupation probabilities that run on the single-particle states of the two fragments are preserved. The solutions $\rho_{k(\gamma)}$ and $\kappa_{k(\gamma)}$ are obtained up to an internuclear distance of $R = 22$ fm. The calculated values of $\bar{E}_\gamma$ and $T_{k\gamma}$ as function of R are recorded and will be used later to solve Eqs. (12)–(16). For the two isospins and for all velocities and seniority configurations involved, the systems are solved within the Runge–Kutta algorithm. The dissipated energies E^* after the scission as function of the internuclear velocity v, computed according to Eqs. (19) and (20), are plotted in Fig. 6 for the seniority-zero and the lower single-particle excitation seniority-two states. The general trend exhibited in both cases is an increase of the final dissipated energy when the internuclear velocity becomes larger. The same behavior is typical for all seniority configurations involved. So the general rule that assesses that the dissipation is proportional to the velocity is retrieved. Another way to introduce the dissipation in quantum systems is to consider forces proportional to the velocity in analogy with the friction forces in classical mechanics [53], leading to a generalized Schrödinger nonlinear equation for an open system.

The initial condition for Eqs. (12)–(16) that describe the configuration mixing is $P_0 = 1$, all the other values being zero. From physical considerations, we imposed in the numerical code the conditions that $\dot{P}_{ij} \leqslant 0$ if $P_{ij} = 1$ or if $P_0 = 0$, and that $\dot{P}_{ij} \geqslant 0$ if $P_{ij} = 0$ or if $P_0 = 1$. That ensures that the probability to have any configuration must be in the interval $[0,1]$. The final probabilities of realization of two configurations for neutrons and protons as function of the internuclear velocities are displayed in Fig. 7. This figure evidences the fact that the probability of realization of adiabatic seniority-zero states are close to zero for small velocities, exactly in the energy region in which the dissipation is smaller. So, the main features concerning the relation between the final excitation energy and the probability of realization of a given channel presented in Ref. [4] are retrieved and are valid even if the method for dynamical projection on final atomic and mass numbers is used. The saddle-to-scission time τ depends on the intrinsic velocity v. This scission time τ labels the upper axis of Fig. 7.

The results concerning the final excitation and the probabilities of realization presented above are coupled through the collective velocity parameter. In order to compare the theoretical findings with the experimental data, this velocity must be eliminated. Therefore, a simple model related to the experimental arrangement is conceived in order to relate the dissipation and the yields. By bombarding the ^{233}U with thermal neutrons and using mass evaluations [54] we found that an excitation of at least $B_n = 6.85$ MeV is accumulated in the compound ^{234}U nucleus. As represented in Fig. 3, this energy is shared between a potential part U and a kinetic one $T = 2B_0v^2/2$, where B_0 is the inertia in the ground-state configuration. A constant population of all values of the kinetic energy is assumed. The penetrability $P_b(v,\gamma_n,\gamma_p)$ of each channel depends on the turning points of the barrier; that is, on v through the relation $B_n = U + T$. That leads to a larger penetrability when the velocity decreases. The penetrability depends also on the excitation channel $\{\gamma\}$ that can be constructed with the specialization energies of the configurations $\{0\}$ or $\{ij\}$ of the two isospins. The final excitation energy of the two fragments is $E^*_x(v,\gamma_n,\gamma_p) = E^*(v,\gamma_n,\gamma_p) + E_{sp}(\gamma_n,\gamma_p)$; that is, it corresponds to a sum

between the dissipated energy E^* and the single-particle excitations E_{sp} of the two fragments. The dependence of the yield as function of the final excitation E_x^* in the interval $[E_{x1}^*, E_{x2}^*]$ exhibits the following proportionality:

$$Y_0(E_x^*) \propto \frac{1}{E_{x2}^* - E_{x1}^*} \int_0^{v_{\max}} \Big[P_{0(n)}(v) P_{0(p)}(v) P_b(v,0,0) + P_{0(n)}(v) \sum_{\gamma_p} P_{\gamma_p(p)}(v) P_b(v,0,\gamma_p) + P_{0(p)}(v) \sum_{\gamma_n} P_{\gamma_n(n)}(v) P_b(v,\gamma_n,0) + \sum_{\gamma_n,\gamma_p} P_{\gamma_n(n)}(v) P_{\gamma_p(p)}(v) P_b(v,\gamma_n,\gamma_p) \Big] \times w(v)\theta(E_{x1}^* - E_x^*(v,\gamma_n,\gamma_p)) \times \theta(E_x^*(v,\gamma_n,\gamma_p) - E_{x2}^*) dv, \quad (22)$$

for the even-even channel. Here, P_b are the penetrabilities that depend on a specific channel and P_0 are the probabilities of realization given by the time-dependent equations for neutrons [index (n)] and protons [index (p)]. For all velocities that give an excitation in the interval $[E_{x1}^*, E_{x2}^*]$, the previous formula reflects the fact that the yields are proportional to these penetrabilities and probabilities. Of course, at scission it is possible to obtain even-even partitions even if a Cooper pair is broken. In this case, one of the fission products picks this broken pair and will carry a very large excitation energy. Therefore, the sums that run over the channels γ in Eq. (22) take into consideration the fact that some configurations are formed with a broken pair in only one partner. The probabilities of realization of a given seniority configuration $P_{\gamma_n(p)}(v)$ depend on the internuclear velocity. The penetrability of the fission barrier $P_b(v,\gamma_n,\gamma_p)$ at the velocity v in the channel $\{\gamma_n,\gamma_p\}$ depends on the variation of the probabilities of realization along the fission path. The factor $w(v) = B_0 v$ is a weighting that reflects the dependence of the kinetic energy of the velocity, because $dT = w(v)dv$, and θ is the step Heaviside distribution used to select only events in the interval $[E_{x1}^*, E_{x2}^*]$. B_0 is considered to be the inertia in the ground state of the parent nucleus. The maximal value of the the velocity is obtained from the boundary $T_{\max} = \frac{1}{2} B_0 v_{\max}^2 = B_n$. The penetrability $P_b(v,\gamma_n,\gamma_p)$ is calculated by considering the turning points at the energy $U = B_n - \frac{1}{2} B_0 v^2$. The calculations were made within three approximations for the inertia: the cranking model [5], the Gaussian overlap approximation [49,50] and the nonadiabatic cranking approach [47,48]. The yields for odd-odd partitions are proportional:

$$Y_2(E_x^*) \propto \frac{1}{E_{x2}^* - E_{x1}^*} \int_0^{v_{\max}} \sum_{\gamma_n} \sum_{\gamma_p} P_{\gamma_n(n)}(v,) P_{\gamma_p(p)}(v,) \times P_b(v,\gamma_n,\gamma_p) w(v) \theta(E_{x1}^* - E_x^*(v,\gamma_n,\gamma_p)) \times \theta(E_x^*(v,\gamma_n,\gamma_p) - E_{x2}^*) dv. \quad (23)$$

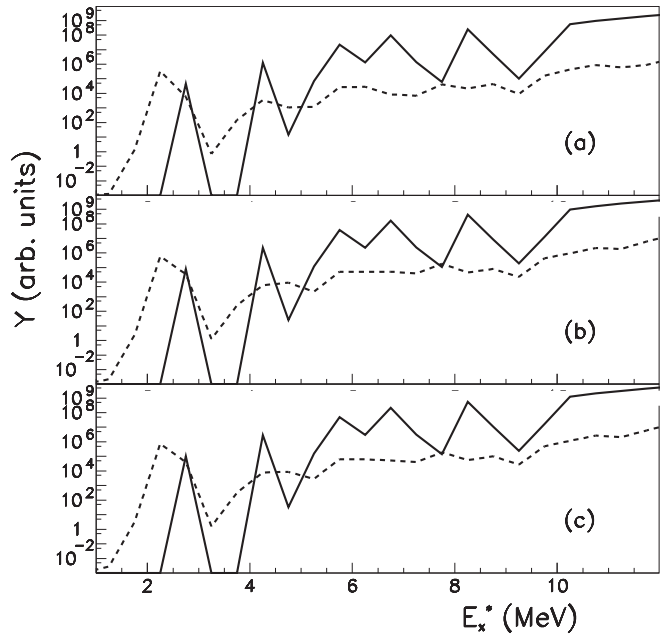

FIG. 8. Full line: dependence of even even yield in arbitrary units Y_0 as function of the final excitation E_x^* of the fission fragments. Dashed line: dependence of the odd-odd yields Y_2 as function of the excitation energy. Panel (a) corresponds to the cranking model, panel (b) is obtained with the nonadiabatic cranking approach, and panel (c) is obtained with the Gaussian overlap approximation.

In the previous relationship, the sums run over all the seniority-two configurations taken into consideration for neutrons (index n) and protons (index p) that give unpaired nucleons in the two fragments.

The results obtained for the folded distributions $Y_0(E_x^*)$ and $Y_2(E_x^*)$ are displayed in Fig. 8. The averaging interval is $E_{x2}^* - E_{x1}^* = 0.5$ MeV. The observed experimental trends exhibited in Fig. 4 of Ref. [1] for cold fission yields were reproduced. The trends are same for the three approaches used for the inertia. At low excitation energy the odd-odd yields surpass the even-even ones. The even-even yields become larger for excitation energies larger that 3 to 4 MeV, in accordance with the experimental findings.

IV. DISCUSSION AND CONCLUSIONS

In this work, a microscopic model is proposed for the explanation of the odd-even effect in cold fission. This explanation is based on a mixing configuration mechanism that is produced during the fission process. This configuration mixing mechanism is obtained dynamically by solving a the generalized system of time-dependent pairing equations, which include a pair-breaking effect. A first rule can be extracted from this model. The even-even fission products cannot be obtained at zero excitation energies because of the existence of dynamical excitations produced in the avoided-level-crossing regions when the nuclear system deforms slowly.

The magnitudes of the interactions and the location of the the avoided-crossing regions are fixed along the fission path

and are independent of the velocity of passage through these regions. If this velocity is large, the perturbation will act on the Cooper pair a small fraction of the time. So, the chance to break a pair will be small. If the velocity is low, the pairs will traverse the regions in larger time durations. So, the probability to break a pair increases. On another hand, high velocities lead to large dissipation energies.

Another characteristic that was not exploited in this work can be featured from the model. The lower excitation energies of a combination of two odd-odd partners can be obtained only if their spin are the same for neutrons and protons. If the spins of the partners are not the same, the model predicts that at least two pair ruptures are produced for neutrons or protons and additional single-particle excitations must be taken into consideration.

The possibility to jump from one level to another in a large-scale-amplitude motion was predicted by Hill and Wheeler in Ref. [5]. Dissipation in terms of Landau–Zener crossings during fission was first proposed in Ref. [55] where excitations were considered only for time-reversed pairs, neglecting the possible existence of unpaired nucleons. As evidenced in Ref. [56], many studies were performed in order to exploit this mechanism in different types of processes. It was also shown in Ref. [27] that the Landau–Zener mechanism is cached in the time-dependent pairing equations (8) and (12). Pairs undergo Landau–Zener transitions on virtual levels with coupling strengths given by the value of the magnitude of the gap parameter. Anyhow, it is the first time that the dynamical pair-breaking effect was used to explain the odd-even effect in fission. It must be mentioned that a time-dependent microscopic approach to the scission process was described in Ref. [57]. They observed that, for scission time greater than 5×10^{-21} s, the single-particle excitations are negligible. This time, which characterizes the neck rupture, corresponds to a velocity of 10^6 fm/fs in our calculations. A typical value for saddle-to-scission time could be considered as $\tau_s \approx 1.3 \times 10^{-21}$. As plotted in Fig. 6, this value of the scission time is consistent with a total excitation energy of the even-even fragments of about 9 MeV (10 MeV for odd-odd ones). For this value τ_s, the probability to have fully paired partners is close to unity.

The density of single-particle levels increases in the region of the second barrier. Therefore, from the outer saddle to the scission, many avoided-crossing regions are produced and the chance to break a pair is enhanced. Up to the second saddle, the number of avoided-crossing regions is small and the system evolves merely in the seniority-zero configuration. That gives a large penetrability for all channels, the mixing of configurations being produced especially in the outer barrier region.

As mentioned, the basic ingredient of the macroscopic-microscopic model is the nuclear shape parametrization. The fission barrier heights emerge as a mixing between the liquid-drop energy and shell (plus pairing) affects behavior. The behavior of both quantities are strongly dependent of the shape of the nuclear system. It is possible to improve the theoretical description of the fission barriers heights to better reproduce the empirical ones by introducing new shape degrees of freedom. For example, it is known that the axial asymmetry, not included in the model, lower the inner fission barrier in the case of U isotopes. It becomes important to discuss the role of the shape degrees of freedom on the accuracy of the results. The dissipation accumulated in the system is a quantity strongly dependent on the intrinsic structure (as well as the shell effects) and on the history of the system (as well as the inertia). If an axial asymmetry parameter is considered during the passage of the first barrier, the shell effects exhibit smaller values along the least-action path. In this case, a lesser degree of rearrangement of the single-particle levels against the ground-state configuration can be presumed in contrast to the situation of axial symmetry. As a consequence, a smaller amount of dissipation can be expected by traversing the first barrier of the axial asymmetric improved parametrization. On the other hand, as evidenced in Ref. [4], the dissipation obtained in the second well is small in comparison to its value at scission. So, it can be anticipated that the influence of the axial asymmetry is not crucial on the final results. An opposite picture is given by the mass-asymmetry degree of freedom. The variation of the mass asymmetry establishes the asymptotic single-particle configurations during the penetration of the second fission barrier. Consequently, a pronounced rearrangement of the intrinsic structure is produced and the associated value of the dissipation becomes important. It is interesting to note that, for cluster decay, where only few particles are emitted from the parent, the same model gives a dissipation of about only 2 to 3 MeV for an internuclear velocity of 1.4×10^6 fm/fs [21]. It can be concluded that the dissipation is mainly sensitive to the shape degrees of freedom able to produce strong rearrangements of the single-particle levels in the topological description of the fission path.

In this paper, the scission configuration takes in account values for the fragment deformations close to the fundamental ones while the fission path corresponds to cold fission. Therefore, small values of the excitation energy are expected. However, if other deformations of the fragment at scission and a path for more elongated shapes are provided, the same prescriptions can be used to describe the odd-even effect. The dissipated energy depends on the modality in which the microscopic levels are rearranged along the specific fission trajectory. If the deformations at scission differ from the ground-state deformations, the specialization energy and the deformation energy of each fragment increase in magnitude, giving finally larger excitation energies.

From the outer turning point of the fission barrier, the deformation energy decreases abruptly. In terms of our nuclear shape parametrization, the scission is produced when the position of the center of the circle that determines the neck region becomes equal to its radius R_3 ($S = 1$). So, the scission configuration is precisely determined if the dependence between the neck generalized coordinate and the elongation is known. This dependence was deduced from the least-action principle in the region of the fission barrier and was extrapolated for elongations larger than the outer turning point. The scission point was determined in this context. At scission and in the external region, the single-particle diagram of the whole system resembles to a great extent to the superposition of the asymptotic single-particle levels of both fragments. It can be inferred that only minor modifications

of the dissipated energy are produced after scission because the amount of dissipated energy is mainly managed by the variation in time of the single-particle energies. However, for a constant value of the internuclear velocity, the dissipated energy depends on the position of the scission point. If the scission is produced at small values of the elongation, close to the saddle configuration, a sudden rearrangement of the single-particle levels is produced in order to reach the asymptotic intrinsic configurations. In this case, the expected amount of dissipated energy is larger.

In conclusion, by solving the dynamical microscopic equations of motion for a fissioning even-even system it is found that the probability to obtain an odd-odd partition overcomes the probability of an even-even one at excitation energies smaller than 4 MeV, for the same division in mass numbers. The theoretical results are in accordance with the experimental behavior of the odd-even distributions at high kinetic energies. It is the first time that this behavior was explained within a quantum-mechanical approach.

ACKNOWLEDGMENT

This work was supported by CNCS-UEFISCDI, Project No. PN-II-ID-PCE-2011-3-0068.

APPENDIX: EQUATIONS FOR CONFIGURATION MIXING

The following identities are used to develop the functional (6):

$$\left\langle c_0\prod_k(u_{k(0)}+v_{k(0)}a_k^+a_{\bar{k}}^+)\middle|\, H(t)-\lambda|N_2\hat{N}_1-N_1\hat{N}_2|\,\middle|\times c_0\prod_k(u_{k(0)}+v_{k(0)}a_k^+a_{\bar{k}}^+)\right\rangle$$
$$=|c_0|^2\left[2\sum_k|v_{k(0)}|^2\left(\epsilon_k-sN_{i_k}\lambda\right)+\sum_k u_{k(0)}v_{k(0)}\sum_{k'}u^*_{k'(0)}v^*_{k'(0)}G_{kk'}-\sum_k|v_{k(0)}|^4G_{kk}\right], \tag{A1}$$

$$\left\langle\sum_{j,l\neq j}c_{jl}a_j^+a_{\bar{l}}^+\prod_{k\neq j,l}(u_{k(jl)}+v_{k(jl)}a_k^+a_{\bar{k}}^+)\middle|\, H(t)-\lambda|N_2\hat{N}_1-N_1\hat{N}_2|\,\middle|\sum_{j,l\neq j}c_{jl}a_j^+a_{\bar{l}}^+\prod_{k\neq j,l}(u_{k(jl)}+v_{k(jl)}a_k^+a_{\bar{k}}^+)\right\rangle$$
$$=\sum_{j,l\neq j}|c_{jl}|^2\left(2\sum_{k\neq j,l}|v_{k(jl)}|^2\left(\epsilon_k-sN_{i_k}\lambda\right)+\left(\epsilon_j-sN_{i_j}\lambda\right)+\left(\epsilon_l-sN_{i_l}\lambda\right)\right.$$
$$\left.+\sum_{k\neq j,l}u_{k(jl)}v_{k(jl)}\sum_{k'\neq j,l}u^*_{k'(jl)}v^*_{k'(jl)}G_{kk'}-\sum_{k\neq jl}|v_{k(jl)}|^4G_{kk}\right), \tag{A2}$$

where we introduced the sign $s=\mathrm{sgn}(N_2\sum_{k_1}|v_{k_1(\gamma)}|^2-N_1\sum_{k_2}|v_{k_2(\gamma)}|^2)$ in order to have a positive value of the matrix element of the condition (4). In this last relation $\{\gamma\}=\{0\}$ or $\{ij\}$ denotes a configuration. $N_{i_k}=N_2$ or $N_{i_k}=-N_1$ if the state k will belong to the fragment 1 or 2 after the scission, respectively.

For the time derivatives, the following relations are used:

$$\left\langle c_0\prod_k(u_{k(0)}+v_{k(0)}a_k^+a_{\bar{k}}^+)\middle|\frac{\partial}{\partial t}\middle|c_0\prod_k(u_{k(0)}+v_{k(0)}a_k^+a_{\bar{k}}^+)\right\rangle=c_0^*\dot{c}_0+|c_0|^2\sum_k(u_{k(0)}\dot{u}_{k(0)}+v^*_{k(0)}\dot{v}_{k(0)}), \tag{A3}$$

and

$$\left\langle\sum_{j,l\neq j}c_{jl}a_j^+a_{\bar{l}}^+\prod_{k\neq j,l}(u_{k(jl)}+v_{k(jl)}a_k^+a_{\bar{k}}^+)\middle|\frac{\partial}{\partial t}\middle|\sum_{j,l\neq j}c_{jl}a_j^+a_{\bar{l}}^+\prod_{k\neq j,l}(u_{k(jl)}+v_{k(jl)}a_k^+a_{\bar{k}}^+)\right\rangle$$
$$=\sum_{j,l\neq j}\left[c^*_{jl}\dot{c}_{jl}+|c_{jl}|^2\sum_{k\neq j,l}\left(u_{k(jl)}\dot{u}_{k(jl)}+v^*_{k(jl)}\dot{v}_{k(jl)}\right)\right]. \tag{A4}$$

The matrix elements of the time derivatives of the wave functions are neglected because they are considered to be responsible only for the inertia parameter. These matrix elements were investigated in Refs. [47,48], where a relationship between the inertia and the dissipation was revealed. By using the following properties of the creation and annihilation operators:

$$\begin{aligned}\alpha_k a_k^+&=u_k+v_ka_k^+a_{\bar{k}}^+,\quad \alpha_k^+a_{\bar{k}}^+=u_ka_k^+a_{\bar{k}}^+-v_k^*,\\ \alpha_{\bar{k}}a_{\bar{k}}^+&=u_k+v_ka_k^+a_{\bar{k}}^+,\quad \alpha_{\bar{k}}^+a_k^+=-u_ka_k^+a_{\bar{k}}^++v_k^*,\end{aligned} \tag{A5}$$

the next equalities are deduced:

$$\sum_{i,j\neq i} c_0^* c_{ij} = \left\langle c_0 \prod_k (u_{k(0)} + v_{k(0)} a_k^+ a_{\bar{k}}^+) \middle| \sum_{i,j\neq i} \alpha_{i(0)} \alpha_{\bar{j}(0)} \prod_{k\neq i,j} \alpha_{k(0)} a_k^+ a_k \alpha_{k(ij)}^+ \middle| \sum_{j,l\neq j} c_{jl} a_j^+ a_{\bar{l}}^+ \prod_{k\neq j,l} (u_{k(jl)} + v_{k(jl)} a_k^+ a_{\bar{k}}^+) \right\rangle, \tag{A6}$$

and

$$\sum_{i,j\neq i} c_0 c_{ij}^* = \left\langle \sum_{j,l\neq j} c_{jl} a_j^+ a_{\bar{l}}^+ \prod_{k\neq j,l} (u_{k(jl)} + v_{k(jl)} a_k^+ a_{\bar{k}}^+) \middle| \sum_{i,j\neq i} \alpha_{i(0)}^+ \alpha_{\bar{j}(0)}^+ \prod_{k\neq i,j} \alpha_{k(ij)} a_k^+ a_k \alpha_{k(0)}^+ \middle| c_0 \prod_k (u_{k(0)} + v_{k(0)} a_k^+ a_{\bar{k}}^+) \right\rangle. \tag{A7}$$

By using the previous identities, the energy functional (6) reads, eventually,

$$\begin{aligned}
&\langle\varphi| H - i\hbar\frac{\partial}{\partial t} + H' - \lambda(N_2\hat{N}_1 - N_1\hat{N}_2)|\varphi\rangle \\
&= |c_0|^2 \left[2\sum_k |v_{k(0)}|^2 \left(\epsilon_k - sN_{i_k}\lambda\right) - \sum_k u_{k(0)} v_{k(0)} \sum_{k'} u_{k'(0)}^* v_{k'(0)}^* G_{kk'} - \sum_k |v_{k(0)}|^4 G_{kk} \right] \\
&\quad + \sum_{j,l\neq j} |c_{jl}|^2 \left[2\sum_{k\neq j,l} |v_{k(jl)}|^2 \left(\epsilon_k - sN_{i_k}\lambda\right) + \left(\epsilon_j - N_{i_j}\lambda\right) + \left(\epsilon_l - sN_{i_l}\lambda\right) \right. \\
&\quad \left. - \sum_{k\neq j,l} u_{k(jl)} v_{k(jl)} \sum_{k'\neq j,l} u_{k'(jl)}^* v_{k'(jl)}^* G_{kk'} - \sum_{k\neq j,l} |v_{k(jl)}|^4 G_{kk} \right] - i\hbar \left\{ c_0^* \dot{c}_0 + |c_0|^2 \sum_k \frac{1}{2} (v_{k(0)}^* \dot{v}_{k(0)} - \dot{v}_{k(0)}^* v_{k(0)}) \right. \\
&\quad \left. + \sum_{j,l\neq j} \left[c_{jl}^* \dot{c}_{jl} + |c_{jl}|^2 \sum_{k\neq j,l} \frac{1}{2} (v_{k(jl)}^* \dot{v}_{k(jl)} - \dot{v}_{k(jl)}^* v_{k(jl)}) \right] \right\} + \sum_{l,j\neq l}^{n} h_{jl} (c_0^* c_{jl} + c_0 c_{jl}^*) \\
&= |c_0|^2 \bar{E}_0 + \sum_{j,l\neq j} |c_{jl}|^2 \bar{E}_{jl} - \left\{ i\hbar c_0^* \dot{c}_0 + |c_0|^2 \sum_k T_{k(0)} + \sum_{j,l\neq j} \left[i\hbar c_{jl}^* \dot{c}_{jl} + |c_{jl}|^2 \sum_{k\neq j,l} T_{k(jl)} \right] \right\} + \sum_{l,j\neq l}^{n} h_{jl} (c_0^* c_{jl} + c_0 c_{jl}^*),
\end{aligned} \tag{A8}$$

where $\bar{E}_0$ and $\bar{E}_{jl}$ are terms that include the energies E_0 and E_{jl} [given by Eqs. (17) and (18)] of the seniority-zero and the seniority-two configurations, respectively,

$$\bar{E}_0 = 2\sum_k |v_{k(0)}|^2 \left(\epsilon_k - sN_{i_k}\lambda\right) - \sum_k u_{k(0)} v_{k(0)} \sum_{k'} u_{k'(0)}^* v_{k'(0)}^* G_{kk'} - \sum_k |v_{k(0)}|^4 G_{kk} = E_0 - 2\sum_k \rho_{k(0)} sN_{i_k}\lambda, \tag{A9}$$

$$\begin{aligned}
\bar{E}_{jl} &= 2\sum_{k\neq j,l} |v_{k(jl)}|^2 \left(\epsilon_k - sN_{i_k}\lambda\right) - \sum_{k\neq j,l} u_{k(jl)} v_{k(jl)} \sum_{k'\neq j,l} u_{k'(jl)}^* v_{k'(jl)}^* G_{kk'} - \sum_{k\neq j,l} |v_{k(jl)}|^4 G_{kk} + \epsilon_j - sN_{i_j}\lambda + \epsilon_l - sN_{i_l}\lambda \\
&= E_{jl} - 2\sum_{k\neq j,l} \rho_{k(jl)} sN_{i_k}\lambda - sN_{i_j}\lambda - sN_{i_l}\lambda,
\end{aligned} \tag{A10}$$

and T_γ are state-dependent energy terms:

$$\begin{aligned}
T_{k(0)} &= \frac{i\hbar}{2} (v_{k(0)}^* \dot{v}_{k(0)} - \dot{v}_{k(0)}^* v_{k(0)}) = 2|v_{k(0)}|^2 \left(\epsilon_k - sN_{i_k}\lambda\right) - 2G_{kk}|v_{k(0)}|^4 \\
&\quad + \frac{\Delta_{k(0)}^*}{2} \left(\frac{|v_{k(0)}|^4}{(v_{k(0)} u_{k(0)})^*} - v_{k(0)} u_{k(0)} \right) + \frac{\Delta_{k(0)}}{2} \left(\frac{|v_{k(0)}|^4}{v_{k(0)} u_{k(0)}} - (v_{k(0)} u_{k(0)})^* \right),
\end{aligned} \tag{A11}$$

$$\begin{aligned}
T_{k(jl)} &= \frac{i\hbar}{2} (v_{k(jl)}^* \dot{v}_{k(jl)} - \dot{v}_{k(jl)}^* v_{k(jl)}) = 2|v_{k(jl)}|^2 \left(\epsilon_k - sN_{i_k}\lambda\right) - 2G_{kk}|v_{k(jl)}|^4 \\
&\quad + \frac{\Delta_{k(jl)}^*}{2} \left(\frac{|v_{k(jl)}|^4}{(v_{k(jl)} u_{k(jl)})^*} - v_{k(jl)} u_{k(jl)} \right) + \frac{\Delta_{k(jl)}}{2} \left(\frac{|v_{k(jl)}|^4}{v_{k(jl)} u_{k(jl)}} - (v_{k(jl)} u_{k(jl)})^* \right),
\end{aligned} \tag{A12}$$

where the notation Δ_γ defined in Eq. (17) was introduced.

The time-dependent equations are obtained by minimizing the functional (A9); that is, differentiating with respect the independent parameters $v_{k(0)}$, $v_{k(ij)}$, c_0, and c_{jl}, together with their complex conjugates. Equations (8)–(12) were derived in

different ways in Refs. [21,26,27], and it is straightforward to introduce the condition (4). So, we will focus on the derivation of Eqs. (12)–(16), related to the mixing of configurations.

To obtain the derivatives, the following relations must be used:

$$\begin{aligned} &|c_0|^2+\sum_{j,l\neq j}|c_{jl}|^2=1, \quad \frac{\partial}{\partial c_0}\left[|c_0|^2+\sum_{j,l\neq j}|c_{jl}|^2\right]=0, \\ &\dot{c}_0c_0^*+\sum_{j,l\neq j}\dot{c}_{jl}c_{jl}^*=-\dot{c}_0^*c_0+\sum_{j,l\neq j}\dot{c}_{jl}^*c_{jl}, \quad \frac{\partial\dot{c}_0c_0^*}{\partial c_0}=-\dot{c}_0^*, \quad \frac{\partial\dot{c}_{jl}c_{jl}^*}{\partial c_{jl}}=-\dot{c}_{jl}^*. \end{aligned} \tag{A13}$$

The previous conditions ensure that the sum of the probabilities $|c_\gamma|^2$ of all configurations is one.

The first equations are obtained by differentiating with respect c_0 and c_0^*

$$c_0^*\bar{E}_0+i\hbar\dot{c}_0^*-c_0^*\sum_k T_{k(0)}+\sum_{l,j\neq l}h_{jl}c_{jl}^*=0, \tag{A14}$$

$$c_0\bar{E}_0-i\hbar\dot{c}_0-c_0\sum_k T_{k(0)}+\sum_{l,j\neq l}h_{jl}c_{jl}=0. \tag{A15}$$

After multiplying by c_0 the Eq. (A14) and by c_0^* the Eq. (A15) and subtracting we obtain:

$$i\hbar[c_0\dot{c}_0^*+c_0^*\dot{c}_0]=\sum_{l,j\neq l}h_{jl}[c_{jl}c_0^*-c_{jl}^*c_0]. \tag{A16}$$

Similar equations are obtained by differentiating the functional with respect c_{jl} and c_{jl}^*:

$$c_{jl}^*\bar{E}_{jl}+i\hbar\dot{c}_{jl}^*-c_{jl}^*\sum_{k\neq j,l}T_{k(jl)}+h_{jl}c_0^*=0, \tag{A17}$$

$$c_{jl}\bar{E}_{jl}-i\hbar\dot{c}_{jl}-c_{jl}\sum_{k\neq j,l}T_{k(jl)}+h_{jl}c_0=0. \tag{A18}$$

After multiplying by c_{jl} the Eq. (A17) and by c_{jl}^* the Eq. (A18) and subtracting we construct the expression

$$i\hbar[c_{jl}\dot{c}_{jl}^*+c_{jl}^*\dot{c}_{jl}]=h_{jl}[c_{jl}^*c_0-c_{jl}c_0^*]. \tag{A19}$$

In a similar way we determine an exchange term between seniority-zero and seniority-one configurations. We start from the equalities obtained from the identities (A14) and (A17)

$$\begin{aligned} &i\hbar\dot{c}_0c_{jl}^*=c_0c_{jl}^*\bar{E}_0-c_0c_{jl}^*\sum_k T_{k(0)}+\sum_{m,n\neq m}h_{mn}c_{mn}c_{jl}^*, \quad i\hbar\dot{c}_{jl}^*c_0=-c_0c_{jl}^*\bar{E}_{jl}+c_0c_{jl}^*\sum_{k\neq j,l}T_{k(jl)}-h_{jl}c_0c_0^*, \\ &i\hbar\dot{c}_0^*c_{jl}=-c_0^*c_{jl}\bar{E}_0+c_0^*c_{jl}\sum_k T_{k(0)}-\sum_{m,n\neq l}h_{mn}c_{jl}c_{mn}^*, \quad i\hbar\dot{c}_{jl}c_0^*=c_0^*c_{jl}\bar{E}_{jl}-c_0^*c_{jl}\sum_{k\neq j,l}T_{k(jl)}+h_{jl}c_0c_0^*, \end{aligned} \tag{A20}$$

and we construct the expression

$$i\hbar\frac{d(c_{jl}^*c_0)}{dt}=c_0c_{jl}^*(\bar{E}_0-\bar{E}_{jl})+c_0c_{jl}^*\left(\sum_{k\neq j,l}T_{k(jl)}-\sum_k T_{k(0)}\right)+\sum_{\{mn\}\neq\{jl\}}h_{mn}c_{mn}c_{jl}^*+h_{jl}(c_{jl}c_{jl}^*-c_0c_0^*). \tag{A21}$$

Another exchange term is produced between seniority-two states:

$$-i\hbar\dot{c}_{jl}^*=c_{jl}^*\bar{E}_{jl}+c_{jl}^*\sum_{k\neq j,l}T_{k(jl)}+h_{jl}c_0^*, \quad i\hbar\dot{c}_{mn}=c_{mn}\bar{E}_{mn}+c_{mn}\sum_{k\neq m,n}T_{k(mn)}+h_{mn}c_0, \tag{A22}$$

giving eventually the relation

$$i\hbar(c_{jl}^*\dot{c}_{mn}+\dot{c}_{jl}^*c_{mn})=c_{mn}c_{jl}^*(\bar{E}_{mn}-\bar{E}_{jl})+c_{mn}c_{jl}^*\left(\sum_{k\neq m,n}T_{k(mn)}-\sum_{k\neq j,l}T_{k(jl)}\right)+h_{mn}c_0c_{jl}^*-h_{jl}c_0^*c_{mn}. \tag{A23}$$

If the notations (17) are used in the expression (A16), (A19), (A21), and (A23), the time-dependent equations (12)–(16) for the dynamical pair-breaking effect with dynamic projection of number of particles are obtained.

[1] E. Schwab, H.-G. Clerc, M. Mutterer, J. P. Theobald, and H. Faust, Nucl. Phys. A **577**, 674 (1994).
[2] F.-J. Hambsch, H.-H. Knitter, and C. Budtz-Jorgensen, Nucl. Phys. A **554**, 209 (1993).
[3] H.-H. Knitter, F.-J. Hambsch, and C. Budtz-Jorgensen, Nucl. Phys. A **536**, 221 (1992).
[4] M. Mirea, Phys. Lett. B **680**, 316 (2009).
[5] D. L. Hill and J. A. Wheeler, Phys. Rev. **89**, 1102 (1953).
[6] W. N. Reisdorf, J. P. Unik, and L. E. Glendenin, Nucl. Phys. A **205**, 348 (1973).
[7] H. Wohlfarth, W. Lang, H.-G. Clerc, H. Schrader, K.-H. Schmidt, and H. Dann, Phys. Lett. B **63**, 275 (1976).
[8] C. Signarbieux, M. Montoya, M. Ribrag, C. Mazur, C. Guet, P. Perrin, and M. Maurel, J. Phys. Lett. **42**, 437 (1981).
[9] F. Gonnenwein, Phys. Procedia **47**, 107 (2013).
[10] F. Rejmund, A. V. Ignatyuk, A. R. Junghans, and K.-H. Schmidt, Nucl Phys. A **678**, 215 (2000).
[11] V. Avrigeanu, A. Florescu, A. Sandulescu, and W. Greiner, Phys. Rev. C **52**, R1755 (1995).
[12] M. Montoya, J. Phys. **44**, 785 (1983).
[13] H.-G. Clerc, in *Heavy Elements and Related New Phenomena*, edited by W. Greiner and R. K. Gupta (World Scientific, Singapore, 1999), p. 471.
[14] M. Caamano, F. Rejmund, and K.-H. Schmidt, J. Phys. G **38**, 035101 (2011).
[15] B. Jurado and K.-H. Schmidt, EPJ Web of Conferences **62**, 07003 (2013).
[16] P. Armbruster, in *Proceedings of the International Workshop Gross Properties of Nuclei and Nuclear Excitations III*, edited by W. J. Myers (Kleinwalsertal, Austria, 1975), p. 32, *Technische Hochschule Darmstadt* AED-Conf-75-009-000.
[17] H. Nifenecker, C. Signarbieux, R. Babinet, and J. Poitou, in *Proceedings of the Third IAEA Symposium on the Physics and Chemistry of Fission, Rochester, NY, August 13–17, 1973*, Vol. 2 (International Atomic Energy Agency, Vienna, 1974), p. 117.
[18] J. R. Nix, Ann. Rev. Nucl. Sci. **22**, 65 (1972).
[19] J. Y. Park, W. Greiner, and W. Scheid, Phys. Rev. C **21**, 958 (1980).
[20] M. Mirea, Phys. Rev. C **63**, 034603 (2001).
[21] M. Mirea, Phys. Rev. C **78**, 044618 (2008).
[22] M. Mirea, Mod. Phys. Lett. A **18**, 1809 (2003).
[23] M. Mirea, Int. J. Mod. Phys. E **21**, 1250035 (2012).
[24] M. Mirea, Phys. Rev. C **83**, 054608 (2011).
[25] M. Mirea, Phys. Lett. B **717**, 252 (2012).
[26] S. E. Koonin and J. R. Nix, Phys. Rev. C **13**, 209 (1976).
[27] J. Błocki and H. Flocard, Nucl. Phys. A **273**, 45 (1976).
[28] B. Avez, C. Simenel, and Ph. Chomaz, Phys. Rev. C **78**, 044318 (2008).
[29] S. Ebata, T. Nakatsukasa, T. Inakura, K. Yoshida, Y. Hashimoto, and K. Yabana, Phys. Rev. C **82**, 034306 (2010).
[30] M. Mirea, L. Tassangot, C. Stephan, and C. O. Bacri, Nucl. Phys. A **735**, 21 (2004).
[31] W. J. Swiatecki and S. Bjornholm, Phys. Rep. **4**, 325 (1972).
[32] M. Brack, J. Damgaard, A. S. Jensen, H. C. Pauli, V. M. Strutinsky, and C. Y. Wong, Rev. Mod. Phys. **44**, 320 (1972).
[33] M. Mirea, Phys. Rev. C **54**, 302 (1996).
[34] M. Mirea, Nucl. Phys. A **780**, 13 (2006).
[35] M. Mirea, A. Sandulescu, and D. S. Delion, Proc. Rom. Acad. Series A **12**, 203 (2011).
[36] M. Mirea, A. Sandulescu, and D. S. Delion, Nucl. Phys. A **870**, 23 (2011).
[37] M. Mirea, A. Sandulescu, and D. S. Delion, Eur. Phys. J. A **48**, 86 (2012).
[38] M. Mirea, Rom. J. Phys. **57**, 372 (2012).
[39] A. Sandulescu and M. Mirea, Rom. Rep. Phys. **65**, 688 (2013).
[40] A. Sandulescu, M. Mirea, and D. S. Delion, Europhys. Lett. **101**, 62001 (2013).
[41] M. Mirea, D. S. Delion, and A. Sandulescu, Phys. Rev. C **81**, 044317 (2010).
[42] M. Mirea and L. Tassan-Got, Cent. Eur. J. Phys. **9**, 116 (2011).
[43] A.-M. Micu and M. Mirea, Rom. J. Phys. **58**, 939 (2013).
[44] M. Mirea, D. S. Delion, and A. Săndulescu, Europhys. Lett. **85**, 12001 (2009).
[45] J. A. Wheeler, in *Niels Bohr and the Development of Physics*, edited by W. Pauli, L. Rosenfeld, and W. Weisskopf (Pergamon Press, London, 1955), p. 163.
[46] J. Randrup and P. Moller, Phys. Rev. Lett. **106**, 132503 (2011).
[47] M. Mirea and R. C. Bobulescu, J. Phys. G **37**, 055106 (2010).
[48] M. Mirea, Rom. Rep. Phys. **63**, 676 (2011).
[49] A. Gozdz, K. Pomorski, M. Brack, and E. Werner, Nucl. Phys. A **442**, 26 (1985).
[50] A. Gozdz, K. Pomorski, M. Brack, and E. Werner, Nucl. Phys. A **442**, 50 (1985).
[51] M. Mirea, L. Tassan-Got, C. Stephan, C. O. Bacri, and R. C. Bobulescu, Phys. Rev. C **76**, 064608 (2007).
[52] W. Greiner, J. Y. Park, and W. Scheid, *Nuclear Molecules* (World Scientific, Singapore, 1995).
[53] A. Sandulescu and H. Scutaru, Ann. Phys. **173**, 277 (1987).
[54] G. Audi, A. H. Wapstra, and C. Thibault, Nucl. Phys. A **729**, 337 (2003).
[55] G. Schutte and L. Wilets, Z. Phys. A **286**, 313 (1978).
[56] R. W. Hasse, Rep. Prog. Phys. **41**, 1027 (1978).
[57] M. Rizea and N. Carjan, Nucl. Phys. A **909**, 50 (2013).